Jetting and Detonation Initiation in Shock Induced Collapse of Nanometer-Scale Voids

Yunfeng Shi* and Donald W. Brenner

Department of Materials Science and Engineering, North Carolina State University, Raleigh, North Carolina 27587-7907

Received: December 20, 2007; In Final Form: February 7, 2008

Molecular dynamics simulations have been used to characterize the dynamics of the shock-induced asymmetric collapse of nanometer-scale voids in cubane nitrogen and to characterize how this dynamics couples with local chemistry to increase the shock sensitivity relative to homogeneous initiation. Mesoscopic-scale features of the void collapse correspond well to experimentally observed features of micrometer-scale bubble collapse, including a transition from single to double jetting with an increasing transverse void length. An analytic model is developed for the enhanced shock sensitivity as a function of void size and shape that reproduces the simulation results. At the atomic level, the simulations show vibrational up-pumping of molecules in the jet front because of collisions with the downstream wall followed by bi-molecular reactive dynamics from continued jet impact that triggers the onset of initiation. These results provide important new insights into the coupling of hydrodynamic void collapse and the enhanced shock sensitivity of energetic materials.

I. Introduction

The sensitivity of solid explosives is enhanced by the presence of voids which, when shocked, lead to hotspots via void collapse.[1,2] The specific mechanism by which void collapse leads to local heating depends on several factors, including the initial size of the void, the strength of the applied shock, and the yield strength and viscosity of the shocked solid.[3] Under conditions where the shock travels faster than the characteristic time for void collapse, symmetric collapse occurs, and heating comes mainly from visco-plastic dynamics. As the collapse time approaches the time needed for the shock to traverse the void, void collapse becomes asymmetric, and the collapse dynamics evolves from a viscous to a hydrodynamic regime. The collapse in a fully hydrodynamic regime is characterized by the formation of a jet that emerges from the upstream wall of the void.[4,5] This jetting leads to an enhanced focusing of kinetic energy onto the downstream side of the collapsing void. In both the viscous and the hydrodynamic regimes, there is also a contribution from adiabatic heating of gas trapped in the collapsing void, although the magnitude of this contribution is typically small. Enhanced shear banding in the vicinity of a collapsing void may also contribute to hot spot formation and the enhanced sensitivity observed for energetic materials with increasing porosity.

Jetting during shock-induced collapse of millimeter-size voids in gels has been experimentally characterized by Bourne and Field and co-workers using high-speed photography.[1,2,4,5] In these studies, luminescence was observed from the point at which a jet initially impacts the cavity side wall, as well as from two "lobes" that form on either side of the jet after impact. On the basis of the temperature inferred from the intensity of the luminescence and the time scale of the collapse, they suggest that ignition in energetic materials within the hydrodynamic regime results from the high-speed jet impact on the downstream wall and not from the high temperatures in the lobes that form after impact. They also observed the formation of dual jets during the shock collapse of a void within which the upstream wall is initially a flat surface.

Jetting also plays a critical role in other important processes. The Munroe effect in solids, for example, is exploited in the development of shaped charges,[6] and jetting due to bubble collapse near a solid boundary leads to cavitation erosion.[7]

Several molecular dynamics simulations have provided important insights into the interaction of shocks with nanometer-scale voids in solids that have implications for hotspot formation and shock sensitivity. Mintmire et al. modeled the collapse of a cylindrical void with a 2 nm diameter in a shocked molecular solid composed of harmonic diatomic molecules bound into a solid by pair additive Morse potentials.[8] They reported a transition from symmetric to asymmetric void collapse with increasing speed of the supported shock. For asymmetric collapse, turbulent ejection of molecules into the void followed by collisions with the downstream side of the void was reported which leads to formation of a hotspot. Jetting dynamics, however, was not noted, and because of the nonreactive nature of the interatomic potential, chemical reactivity and shock sensitivity could not be quantified. In subsequent work, White and co-workers modeled the interaction of a driven planar shock with an infinite gap (created via periodic boundary conditions) within a model two-dimensional reactive system.[9] For a gap width of 15 nm, they found that a driven shock would initiate detonation at a front velocity that was 20% below that needed to initiate detonation in a defect-free system. For the detonating system, initiation was not observed at the point at which molecules that were ejected into the void impacted the far side of the gap, but rather initiation occurred as the gap collapsed under the influence of the supported shock. To explain this result, Holian et al. developed a model that considers PV work coming from recompression of the ejected particles.[10] This model predicts size-dependent sub-threshold detonation with chemical reactions initiating in the compressed region, consistent with the White et al. simulations as well as with comparable simulations using a nonreactive Lennard-Jones potential.

* Corresponding author.

10.1021/jp7119735 CCC: $40.75
Published on Web 03/29/2008

Molecular dynamics simulations by Germann et al. used the same model as White and co-workers to characterize shock dynamics and initiation in a two-dimensional system containing circular and elliptical voids.[11] They reported hydrodynamic jet formation and detonation initiation from supported shock fronts that have speeds below that needed to initiate a defect-free system. For elliptical voids, structures having the long axis along the direction of the shock were found to have lower threshold shock pressures than voids with the same shape but with the long axis oriented perpendicular to the shock front. For all cases, initiation was reportedly not a result of the initial jet collision with the downstream wall, but rather chemical reactivity leading to initiation occurred in the high temperatures and pressures during void collapse after the initial jet impact. The lower threshold for elliptical voids with the long axis along the shock direction was attributed to the longer transit time for the jet and therefore the higher PV work available to induce reactivity.

Hatano used molecular dynamics simulations and a nonreactive Lennard-Jones potential to model collapse of nanometer-scale rectangular voids in a solid due to a supported shock.[12] The voids had dimensions from 4 to 40 unit cells. He reported an elevated kinetic energy and an increased number of energetic collisions during collapse. The kinetic energy enhancement was reportedly due to momentum and energy focusing from the two void walls that were along the direction of the supported shock, although no jetting was reported.

Nomura et al. used molecular dynamics simulations and the ReaxFF many-body reactive potential energy expression to model the collapse of a spherical void in an RDX crystal.[13] Because of the computational demands of the potential energy expression and the required system sizes, only two piston speeds were used, 1 km/s and 3 km/s. They observed the formation of a jet that was accelerated through the void due to focusing from the void walls. For the higher piston speed, they report the formation of molecular NO_2 fragments at the jet-sidewall interface as the jet traverses the void. Upon impact of the jet, different products form, most notably N_2, H_2O, and HONO, from mechanisms that included molecular dissociation and recombination. Hence, these simulations provide clear evidence that jetting in a nanometer-scale void can have a large influence on the shock chemistry of energetic materials. However, simulations of RDX using this force field have yet to demonstrate a transition from reactive chemistry to a chemically sustained detonation, and therefore it is difficult to draw further conclusions regarding the role of voids in determining the sensitivity of RDX and related systems from these simulations.

For continuum level analyses, the choice of spherical voids is due to both the ease of computation and the minimum energy shapes assuming isotropic surface free energies. At the nanometer scale, however, faceting that reflects the relative stabilities of discrete surfaces can, in principle, produce voids with relatively abrupt features. The experimental observation of dual jetting during the collapse of macroscopic voids with a flat surface together with the work of Hatano at the atomic scale suggests that such features may play an important role in energy focusing during hydrodynamic collapse. To further explore this issue within the context of detonation initiation, we have carried out an extensive set of molecular dynamics simulations of a supported shock traveling through a reactive system containing nanometer-scale rectangular voids of different sizes and aspect ratios. As described in more detail below, these simulations display characteristics that mimic those observed at the macroscopic scale, including enhanced sensitivity relative to homogeneous detonation, asymmetric collapse and jetting, formation of hot regions of material surrounding the jet impact site, a transition from single to double jetting with increasing transverse void size, and initiation from the point where the jet impacts the downstream void wall. By using these results as a guide, an analytic model is developed that reproduces the influence of void shape on the detonation sensitivity of the material. The simulations are also characterized in terms of reactive chemistry at the atomic scale. The simulations show vibrational up-pumping of spalled molecules due to collision with the downstream wall, followed by a bimolecular reaction with additional spalled molecules that leads to product formation and detonation initiation.

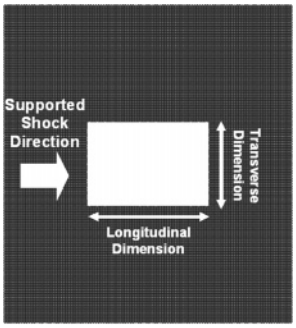

Figure 1. Illustration of the initial simulation system.

II. Simulation

The energetic material used in these simulations was a model nitrogen cubane crystal. A recently developed reactive state summation (RSS) potential was used to model the nitrogen−nitrogen interactions.[14] This potential is designed to model the exothermic dissociation of nitrogen cubane molecules into diatomic nitrogen molecules, and it has been tested in thermal decomposition and mechanical shock simulations in three-dimensional systems.[14] It has been demonstrated that this model has a well-defined threshold for homogeneous detonation via mechanical loading, and steady-state detonation fronts have been observed to propagate at an intrinsic speed. Both of these attributes are critical for studying shock sensitivity via molecular simulation. This energetic material model has also been used to simulate a plastic bonded explosive.[15] The initial configuration of the system used in the current study was a thin slab geometry in which nitrogen cubane molecules were packed in a simple cubic structure in a simulation box of $46 \times 52 \times 0.9$ nm^3. The system was periodic in the Y and Z directions and shocks propagated along the positive X direction. The classical dynamics were calculated using a standard numerical integrator without temperature or pressure control using a time step of 0.08 fs. This relatively small time step was essential to ensure integration stability under the high temperatures associated with detonation process. For all systems, the initial temperature was 0 K (although the system is mechanically stable at finite temperatures).

Rectangular voids were created by removing nitrogen cubane molecules from a perfect crystal (Figure 1). The relevant characteristics of the void are a longitudinal length (X direction) and a transverse length (Y direction). The void dimension in the Z direction was infinite due to the periodic boundary condition. The onset of detonation within a simulation is defined to occur when the total potential energy of the system as it is being shock-compressed starts to decrease relative to the initial state because of the formation of reaction products. Previous studies have demonstrated that these conditions lead to a steady-state detonation in this model. The reaction products include

oligomeric intermediates, N_2, and a very small amount of single nitrogen atoms. For the discussion below, a reaction product is defined as an atom with a potential energy less than −3.0 eV (for reference, N_2 has a potential energy of −4.91 eV/atom and N_8 cubane has a potential energy of −2.41 eV/atom with this potential). A supported shock was generated by keeping the relative positions of the molecules in a single layer rigid and incrementing their positions by a constant amount in the shock direction. To determine relative sensitivities, a series of simulations for each atomic configuration were carried out where each consecutive simulation uses a higher piston velocity until the configuration detonates.

Two series of simulations were conducted, one in which the transverse length of the void was varied while keeping a constant longitudinal length, and one in which the longitudinal length was varied while keeping a constant transverse length (see Figure 1). To evaluate the influence of the placement of the void in the direction of the supported shock, three types of voids within the former series were initially evaluated, a void aligned within 10 nm of the piston, a void aligned within 10 nm of the end of the simulation cell, and a void in the center of the system. The detonation thresholds for the centered void and the void nearest the end of the simulation away from the shock overlap within the uncertainty of the simulation. For longitudinal lengths less than about 15 nm, voids aligned near the piston exhibit a lower detonation threshold than the other systems. For this alignment, as the ejected energetic molecules hit the downstream wall, a compressive re-shock wave is reflected back, and detonation occurs when this re-shock wave reaches the rigid piston. This type of sub-threshold detonation is a result of the finite thickness of the upstream-wall and is thus an artifact of the simulation size. If simulations where the detonation starts at the piston are excluded, the detonation thresholds become independent of the placement of the voids in the direction of the piston motion. Therefore, the remainder of the results are based on center aligned voids. The influence of the system size in the *Z* direction on the threshold piston velocity for detonation was also explored by doubling the thickness of a system containing a void 14 nm in the longitudinal direction and 20 nm in the transverse direction. The threshold velocity was only 2% less than that of the smaller system size, which is within the numerical uncertainty inherent to the simulations of the piston threshold estimates for each void dimension.

III. Results

The discussion of the simulation results is divided into two subsections, one in which void collapse and jetting is discussed, and one in which reactive chemical dynamics is discussed. Because it is established from other studies (see above) that jetting can occur across multiple length scales, the void collapse and jetting observed in these simulations is referred to as mesoscopic-scale dynamics (although the simulations are strictly atomistic). The reactive dynamics, in contrast, is characterized on a molecular level and is therefore referred to as atomic-scale dynamics. The initiation of the detonation wave depends on the coupled dynamics of both scales and is therefore discussed in both of the subsections below.

III.i. Mesoscopic-Scale Dynamics. Plotted as the points (with error bars) in the top panel of Figure 2 are the threshold piston velocities obtained from the molecular dynamics simulations as a function of the transverse length of the void with a constant longitudinal length of 20 nm. The upper bound of the error bar denotes the lowest attempted piston velocity for which the system detonated. The lower bound to the error bar denotes the highest attempted piston velocity that did not detonate the system. For reference, the piston velocity needed for homogeneous detonation of this system is 1.56 km/s. For voids with a longitudinal dimension of 1 nm or less, which are 1 to 2 molecules wide, there is no appreciable reduction in the threshold piston velocity compared with the homogeneous case. In contrast, starting at about 2 nm, there is an approximately 25% reduction in the threshold piston velocity. The threshold velocity increases monotonically for transverse lengths between about 6 and 20 nm, after which the reduction in the threshold piston velocity becomes independent of the transverse length. The points in the bottom panel of Figure 2 are the threshold piston velocities obtained from the molecular simulations as a function of the longitudinal length of the void with a constant transverse length of 14 nm. This transverse length corresponds to the value of the transverse void dimension where the threshold piston velocity begins to increase monotonically with increasing transverse length. As the longitudinal length decreases from 20 nm, the threshold piston velocity increases monotonically until about 8 nm, where there is no longer any appreciable reduction in the threshold piston velocity compared with a homogeneous detonation.

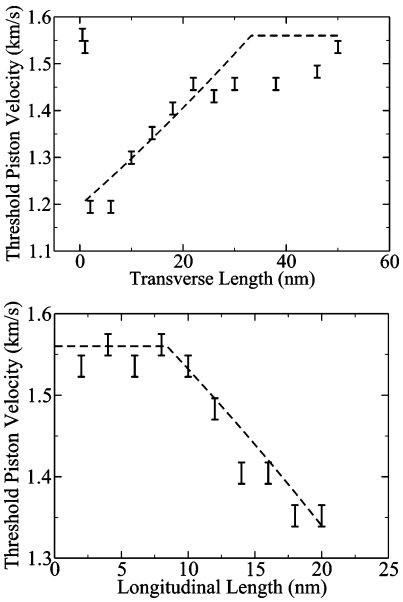

Figure 2. Threshold piston velocities as a function of void dimension. Top panel: data for a constant longitudinal dimension of 20 nm with a varying transverse dimension. Bottom panel: data for a constant transverse dimension of 14 nm and a varying longitudinal dimension. The bottom and top of the error bars denote the highest piston velocity where detonation did not occur and the lowest piston velocity that initiated detonation, respectively. The dashed line is the fit of equations 5a,b to the simulation results.

Illustrated in Figure 3 are a series of snapshots from simulated void collapses for transverse and longitudinal void dimensions of 14 and 20 nm, respectively. The atoms are shaded according to the local effective temperature, and the times are given relative to the time at which the leading edge of the supported shock first reaches the void. The local effective temperature is calculated from the internal kinetic energy of each cubane molecule. Consistent with a hydrodynamic regime, the collapse of the void occurs on the time scale of the passage of the supported shock. Material is ejected into the void as the supported shock front reaches the upstream wall of the void. After a delay, a single jet of material forms that moves through the void until it collides with the downstream wall. After collision, two “lobes” containing a hot gas form on either side

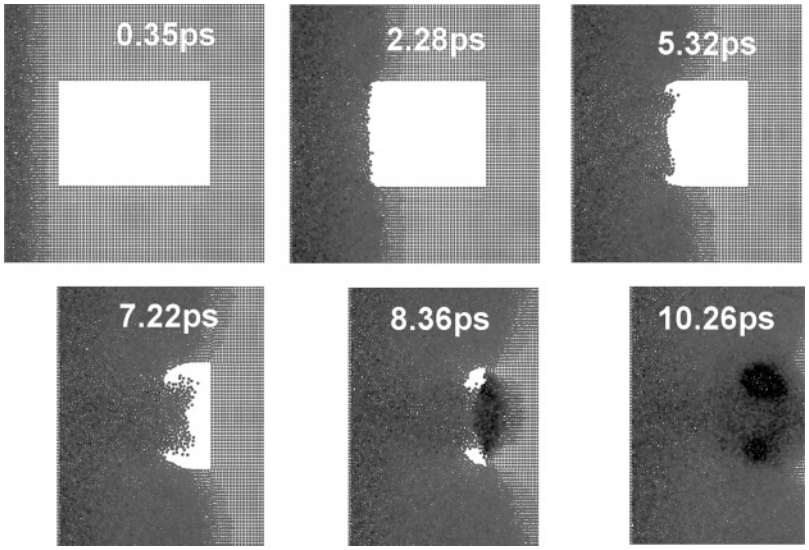

Figure 3. Illustration from a simulation of the hydrodynamic collapse of a void of 20 nm in the longitudinal direction and 14 nm in the transverse direction. The supported shock, which travels from left to right, has a piston velocity just above that needed for initiation. The gray scale corresponds to the internal kinetic energy of each nitrogen cubane. Gray represents 0 eV/atom, and black represents 0.4 eV/atom. The times are relative to that at which the supported shock first reaches the void.

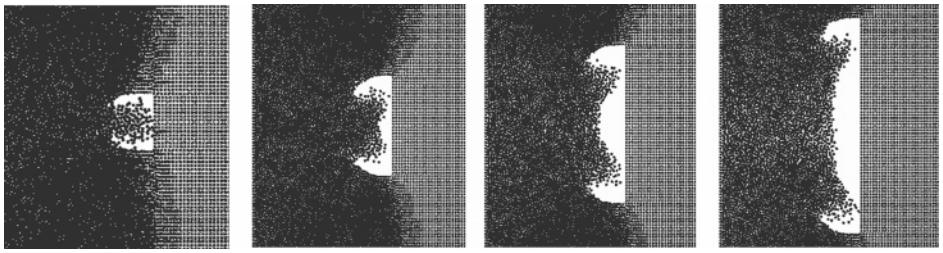

Figure 4. Snapshots from simulations as the jet impacts the downstream void wall for different transverse void lengths with the same longitudinal length (20 nm). The transverse lengths are 6, 14, 22, and 30 nm from left to right.

of the jet impact point. The formation of these lobes is consistent with the experimental high-speed photography images and luminescence studies of the hydrodynamic collapse of millimeter-size cylindrical voids in gels by Bourne and Field and co-workers discussed above.[1,2,4,5] Hence, the shape and heating profile in these atomic-scale simulations are qualitatively consistent with those observed experimentally at the macroscopic scale.

The increase in the threshold piston velocity with respect to the transverse void size apparent from the bottom panel of Figure 2 can be qualitatively understood by further examining the mesoscopic-scale dynamics of the void collapse. Illustrated in Figure 4 are snapshots of systems just prior to the impact of material onto the down stream portion of the void for different transverse void lengths that correspond to those in the top panel of Figure 2. In the region with the lowest threshold piston velocity, there is a single jet that is focused by both walls of the void. As the transverse length increases with a constant longitudinal length, the focusing effect of the two walls is diminished, and the jet is correspondingly more diffuse. With further increase in the transverse void dimension, the hydrodynamic collapse evolves to two jets, each of which is focused by only one wall. Once these two jets become sufficiently isolated from one another, the threshold piston velocity for detonation becomes independent of transverse length. The production of dual jets from two corners of a collapsing void is consistent with the macroscopic-scale experiments by Bourne and Field and co-workers discussed above.

In the final stages of the hydrodynamic void collapse illustrated in Figure 3, material flows into the two lobes on either side of the jet both from the region of the jet impact and from the collapsing walls of the initial void. Hence, the entire void collapse process can be considered as a primary collapse from jetting and secondary collapsing of the lobes. Because of the geometry of the system, material flows into the lobes from the direction of the jet impact and from the direction of the void walls; hence, this secondary collapse is more symmetric than the primary collapse that is accompanied by jetting. In the case of double jetting, there is also a secondary void collapse into lobes formed between the jets and the initial void walls, as well as an additional secondary void collapse in the region between the two jet impact points. This is visible in the double jetting snapshot in Figure 4. For the simulation conditions used here, the material that enters the void formed between the jets comes from the upstream direction, and hence, the secondary collapse in the center of the system is asymmetric, although an additional jetting is not observed.

Plotted in the top panel of Figure 5 is the average velocity of 10 molecules that define the leading edge of the material ejected into the void as a function of time for the system corresponding to the dynamics illustrated in Figure 3. The time in the plot is relative to the time at which the supported shock first reaches the upstream void wall. Plotted as the solid line in the bottom panel of Figure 5 is the position of the same 10 molecules as a function of time during the collapse of the void for the same system. The ejected material undergoes a rapid acceleration over approximately 0.5 ps to a constant velocity of $\sim$1.2 km/s, which roughly matches the piston velocity of 1.36 km/s. During this time, the material in the void has ejected en masse in a compressed state reminiscent of the bulk material

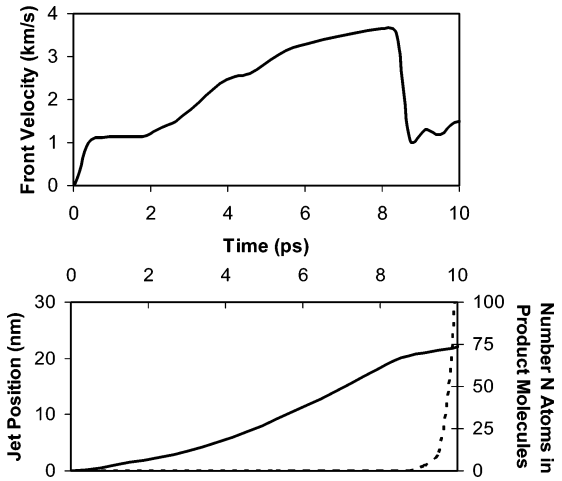

Figure 5. Data from the simulation illustrated in Figure 3. Top Panel: jet front velocity as a function of time. Bottom Panel: jet front position (solid line) and number of nitrogen atoms in the products in the system (dashed line) as a function of time. The time in both panels are relative to that at which the shock front first reaches the upstream void wall. The jet front position is relative to the upstream edge of the void.

in the front of the supported shock. Starting at about 2 ps, the ejected material decompresses, which results in a further acceleration to roughly twice the piston velocity at about ~4 ps. This primary acceleration is consistent with the observations of Holian and co-workers in their simulations of shocked material containing a void. For times greater than ~4 ps, the ejected material undergoes an additional acceleration that is concurrent with the formation of the jet (see Figure 3). This secondary acceleration, which results from focusing from the walls, is responsible for the reduced threshold piston velocity in the bottom panel of Figure 2 for longitudinal voids greater than ~9 nm. A similar acceleration due to wall focusing was also noted in recent simulations by Numora et al.[13]

By using the concepts gleaned from Figures 2−5, an analytic expression can be derived that reproduces the dependence of the threshold piston velocity on the longitudinal and transverse void lengths as indicated in Figure 2. For simplicity, the primary acceleration is ignored, and it is assumed that the spalled material prior to jet formation has a velocity of $2V_p$ where V_p is the piston speed. This approximation is justified by the behavior indicated in the bottom panel of Figure 2, which demonstrates that during the period over which the ejected material is decompressing the threshold piston velocity is constant. Apparently, the total energy of the ejected material, not just the kinetic energy, contributes to detonation initiation. It is further assumed that, after focusing, the jet front undergoes an additional accelerated a due to focusing by the void walls, but this acceleration is delayed because of the time needed for the decompression wave in the leading edge of the void to propagate to the side walls. The delay time t_d can be estimated as the transverse length W divided by the propagation velocity of the decompression wave V_d

$$t_d = \frac{W}{V_d} \tag{1}$$

With these assumptions the jet front velocity as a function of time t (the time origin being the moment the shock reaches the void) is

$$V_j = 2V_p, \qquad t < t_d \tag{2a}$$

$$V_j = 2V_p + a(t - t_d), \qquad t \geq t_d \tag{2b}$$

and the jet front position x_j with respect to the upstream edge of the void is

$$x_j = 2V_p t, \qquad t < t_d \tag{3a}$$

$$x_j = 2V_p t + \frac{a}{2}(t - t_d)^2, \qquad t \geq t_d \tag{3b}$$

Solving equation 3 for t when $x_j = L$ and substituting in equation 2 gives the jet front velocity when the jet collides with the downstream wall as

$$V_j = 2V_p, \qquad \frac{L}{2V_p} < t_d \tag{4a}$$

$$V_j = \sqrt{4V_p^2 + 2a(L - 2t_d V_p)}, \qquad \frac{L}{2V_p} \geq t_d \tag{4b}$$

Within this model, the threshold piston velocity for detonation of a void V_p^{det} corresponds to the conditions at which the velocity of the ejected material just before reaching the downstream wall of the void equals twice the threshold piston velocity for a perfect crystal $V_p^{crystal}$. Therefore, the threshold piston speed for the voids is

$$V_p^{det} = V_p^{crystal}, \qquad \frac{L}{2V_p^{crystal}} < \frac{W}{V_d} \tag{5a}$$

$$V_p^{det} = \frac{1}{2}\left(\frac{aW}{V_d} + \sqrt{-2aL + a^2\left(\frac{W}{V_d}\right)^2 + 4(V_p^{crystal})^2}\right), \qquad \frac{L}{2V_p^{crystal}} \geq \frac{W}{V_d} \tag{5b}$$

Indicated by the dashed lines in Figures 2 are the relations given by equations 5a,b. The quantity $V_p^{crystal}$ was measured to be 1.56 km/s, leaving two fitting parameters, the jet acceleration a due to focusing from the void walls and the speed for the decompression wave V_d. The best fit to the simulation data corresponds to $a = 0.1 \times 10^{15}$ m/s^2 and $V_d = 5.18$ km/s. The velocity of the decompressive wave is close to the range of the velocity (6.8 to 8.4 km/s) of the shock created by the piston. The analytic expressions equations 5a,b provide an excellent fit to the data in the bottom of Figure 2. However, there are noticeable deviations between the analytic model and the simulation results for the top panel of Figure 2. Equation 2b in the above model only considers the acceleration of ejected material as a whole and does not account for the jet formation nor for the transition from single jet to double jets. Therefore, the delay time t_d is an overestimate because the true acceleration is more localized. This leads to an overestimate of the detonation threshold. This effect is more pronounced for voids with large transverse lengths.

To characterize the possible contribution of recompression to initiation sensitivity for this system, simulations were also carried out for planar voids without sidewalls with gap widths up to 20 nm. In contrast to the simulation results reported in ref 9, no reduction in detonation threshold was found, suggesting that gas recompression without jetting does not make a significant contribution to enhanced sensitivity for this system.

III.ii. Atomic-Scale Dynamics. Plotted in the bottom panel of Figure 5 as the dashed line is the number of nitrogen atoms in products in the system as a function of time during void

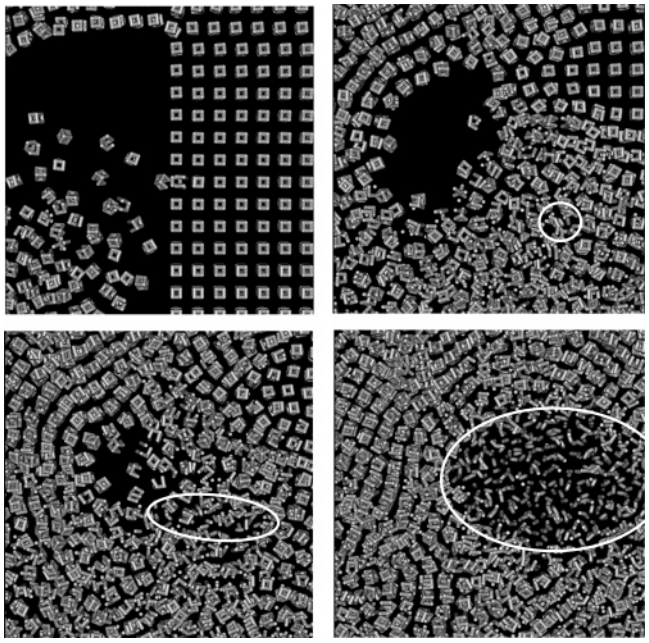

Figure 6. Close-up snapshots of the same system discussed in Figure 3 and Figure 4 near the region where the jet first impacts the void downstream wall.

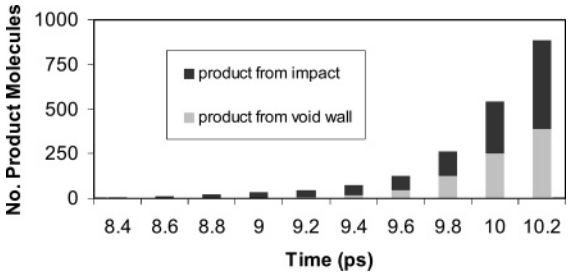

Figure 7. Number of product species arising from different spatial regions of the simulation at different times for the system illustrated in Figure 6.

collapse. No product molecules are formed during the time period over which the jet forms and accelerates through the void. After the jet collides with the downstream wall, products begin to form, with the number of products rising sharply starting at about 9.5 ps or about 1 ps after the jet first collides with the down stream void wall. Illustrated in Figure 6 are snapshots from the simulation corresponding to Figure 5 where only the local region near the initial jet collision with the downstream wall is shown. The products are indicated by circles superimposed over the snapshots. Reactions leading to product molecules initially occur in the condensed region where the jet first impacts the void wall. As the simulation progresses, material expands into the lobes from both the impact region and from the walls of the void, leading to the heating observed on the mesoscopic scale.

Plotted in Figure 7 are the number of product molecules at different times for the simulation illustrated in Figure 6. The dark portion of the bars correspond to product species that originated from cubane molecules that were initially part of the jet or part of the downstream void wall near the jet impact point. The lighter portion of the bars correspond to product species that originated from cubane molecules that were initially part of the void wall that expanded in the hot lobes. Prior to 9 ps, all of the product species (a total of 31) originated from the impact dynamics. As the system evolves in time, products start to form in the hot lobes, and by about 9.8 ps, the amount of

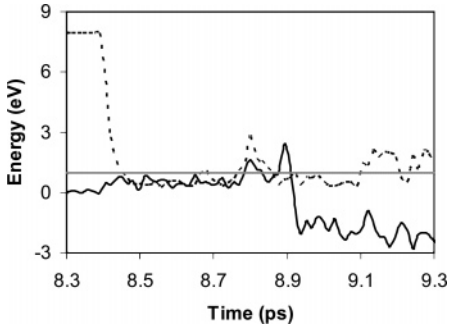

Figure 8. Total center-of-mass kinetic energy (dotted line) and the total potential energy (relative to that at 0 K of an isolated molecule) for a molecule at the jet front from the simulation illustrated in left-most simulation of Figure 4. The horizontal shaded line is the potential energy barrier for thermal reaction (1 eV).

product originating from the side wall molecules match that from the impact. For reference, by using the criteria given above, the onset of detonation occurs at ~9.7 ps. From this data, it is apparent that the exothermic reactions that transition to detonation originate initially from the impact point. Taken together with the ability of the model described above to reproduce the dependence of the threshold piston velocity on void dimensions using only the velocity of the jet front as it traverses the void, this observation suggests that the expansion and subsequent recompression in the lobes is not the primary mechanism that initiates detonation for this system. This conclusion is consistent with the conclusions based on macroscopic-scale experimental studies of void collapse discussed above where initiation arises from the jet impact and not from the hot regions associated with the lobes.

The jet front velocity needed for detonation initiation is ~3.12 km/s, which corresponds to a total center-of-mass kinetic energy of ~8 eV for each cubane molecule. This kinetic energy is significantly larger than the thermal barrier of 1 eV for the formation of N_2 from cubane for the potential model used here,[14] which implies a relatively inefficient transfer of center-of-mass kinetic energy directly to the reaction coordinate during collisions with the downstream void wall. Plotted as the dotted line in Figure 8 is the total center-of-mass kinetic energy for a molecule at the jet front for the simulation illustrated in Figure 6. Plotted as the solid line in Figure 8 is the total potential energy relative to that at 0 K of the same molecule, while the horizontal line indicates the potential barrier of 1 eV for dissociation. The molecule rapidly loses center-of-mass kinetic energy when it hits the downstream void wall at about 8.4 ps. The internal potential energy rises up to about 0.8 eV (which is just below the reaction barrier) at about 8.45 ps, and again at about 8.65 ps. At 8.8 ps, the internal potential energy rises to 1.64 eV, decreases to below 1 eV, and then rises again to 2.45 eV at 8.9 ps after which the potential energy decreases because of the reaction that leads to the formation of N_2.

Plotted in the top panel of Figure 9 is a close-up of the data in Figure 8. To better analyze the dynamics associated with this plot, the data is divided into six regions that are denoted by Roman numerals. In region I, which is before the initial collision with the downstream wall, there is a small oscillation in the potential energy that arises from a vibrational symmetric breathing mode of the molecule. In region II, the molecule in the jet first collides with the downstream wall. The translational kinetic energy declines sharply with a corresponding increase in the internal potential energy. In region III, the molecule continues to vibrate with a greater amplitude. For reference, the gray line from about 8.5 to 8.65 ps corresponds to a squared

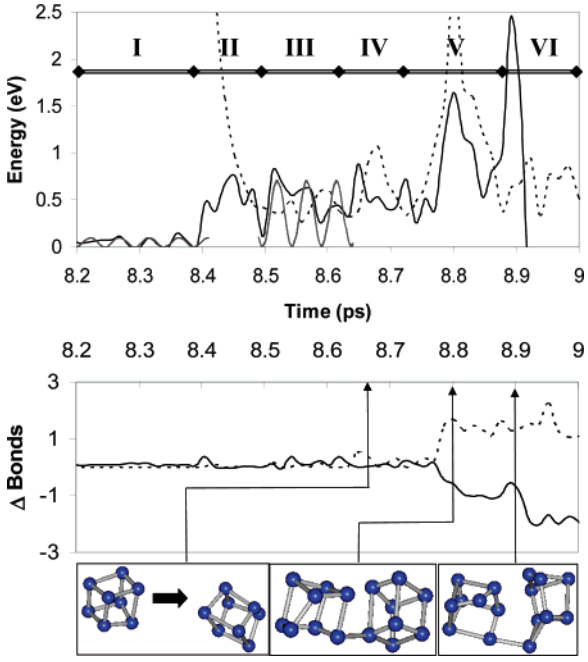

Figure 9. Data from the same simulations discussed in Figure 8. Top Panel: close-up of data in Figure 8. The dotted line, solid line, and gray lines represent the center-of-mass kinetic energy, relative potential energy, and squared sine wave functions, respectively. The Roman numerals correspond to different reaction dynamics. Bottom Panel: the change in the number of bonds within the molecule (solid line) and the number of bonds to the molecule (dotted line). The illustrations at the bottom are for two colliding molecules, and the times are indicated by the arrows.

sine wave with the same frequency as the molecular breathing mode, and that has an amplitude and phase shift that best matches the peaks in the molecular potential energy. This molecular dynamics appears to be an "up-pumping" of the breathing mode due to the collision with the downstream wall. There are second and third collisions of the jet molecule in regions IV and V. The former corresponds to an additional collision with a molecule that was initially in the void wall, while the collision in region V is with a molecule that was further back in the jet that collided with the void wall in the vicinity of the initial jet impact. The latter collision transfers a significant amount of kinetic energy into the molecule that was already vibrationally excited due to the initial jet impact. This combination of impacts is apparently sufficient to initiate the production of N_2 molecules that signal the start of the chemically sustained detonation.

Plotted at the bottom of Figure 9 is the change in the number of bonds associated with the molecule whose energy is tracked in the upper plot as determined by the bond counting function used in the potential energy expression.[14] The solid line corresponds to the change in intramolecular bonds, while the dashed line corresponds to changes in the intermolecular bonds. The images at the bottom of Figure 9 illustrate the dynamics of the molecules of interest at the times indicated by the arrows. In these illustrations, the molecule to the right is the molecule that was initially at the front of the jet, while the molecule at the left of each panel is the molecule that is responsible for the collision in region V in the upper plot. The collisions in regions II and IV in the upper plot do not result in significant changes in the bonding topology. In contrast, the collision with the second molecule in the jet in region V results in the formation of first one and then two intermolecular bonds and the corresponding breaking of one and then two intramolecular bonds. The concerted dynamics leads to the formation of the N_2 products, which release energy with further reaction transitions to the detonation. From this analysis, which is representative of the reactive chemistry in this simulation, the reactive dynamics appear to involve vibrational up-pumping from the initial jet collision followed by a bi-molecular reaction.

The details of reactions such as these will obviously depend very sensitively on the molecular species and the features of the potential energy surface,[13] and therefore, appropriate caution is warranted with respect to drawing general conclusions regarding reaction mechanisms. Nonetheless, this analysis, together with the mesoscopic-scale analysis in the prior section, illustrates the inherent complex interplay between reactive chemistry, hydrodynamic void collapse and jetting, and the initiation dynamics of an energetic crystal.

IV. Conclusions

Molecular dynamics simulations have been used to characterize the dynamics of shock-induced collapse of nanometer-scale voids in cubane nitrogen with different aspect ratios and to characterize how this dynamics couples with local chemistry that transitions to a chemically sustained shock front. Mesoscopic-scale features of the void collapse correspond well to experimentally observed features of micrometer-scale bubble collapse characterized by high-speed photography. These features include asymmetric collapse and jetting with a transition from single to dual jets with increasing transverse dimensions of the void and the formation of hot lobes of material on either side of initial jet impact. The simulations demonstrate initiation from the initial impact rather than from the hot lobes, also in agreement with conclusions made on the basis of prior macroscopic-scale studies. An analytic model is developed for the reduction in the initiation piston threshold as a function of void size and shape that reproduces the simulation results. At the atomic level, the simulations show up-pumping of molecules in the jet front because of collisions with the downstream wall, followed by bi-molecular reactive dynamics from continued jet impact that triggers the onset of detonation. While the system studied here is relatively simple compared with energetic materials of practical interest, these results provide important new insights into the coupling of asymmetric void collapse dynamics and the enhanced sensitivity of energetic materials.

Acknowledgment. We thank D. Thompson, T. Sewell, Y. Hu, and B. Broom for stimulating discussions. This research was supported in part by the National Science Foundation through TeraGrid resources provided by the NCSA. The North Carolina State University High-Performance Computing Facility is also thanked for providing computational resources. The simulations were performed using LAMMPS molecular dynamics software (http://lammps.sandia.gov) with a customized force field. This work was supported by a Multi-University Research Initiative from the U.S. Army Research Office.

References and Notes

(1) Bourne, N. K.; Field, J. E. *Proc. R. Soc. London A* **1999**, *455*, 2411.
(2) Field, J. E. A*cc. Chem. Res.* **1992**, *25*, 489.
(3) Kang, J.; Butler, P. B.; Baer, M. R. *Combust. Flame* **1992**, *89*, 117.
(4) Dear, J. P.; Field, J. E.; Walton, A. J. *Nature* **1988**, *332*, 505.
(5) Bourne, N. K.; Field, J. E. *J. Fluid Mech.* **1992**, *244*, 225.
(6) Waters, W. P.; Zukas, J. A. *Fundamentals of shaped charges*; John Wiley & Sons: New York, 1989.
(7) Kornfield, M.; Suvorov, L. *J. Appl. Phys.* **1944**, *15*, 495.
(8) Mintmire, J. W.; Robertson, D. H.; White, C. T. *Phys. Rev. B* **1994**, *49*, 14859.

(9) White, C. T.; Swanson, D. R.; Robertson, D. H. In *Chemical Dynamics in Extreme Environments;* Dressler, R., Ed.; World Scientific: Singapore, 2001; p 547.

(10) Holian, B. L.; Germann, T. C.; Maillet, J. B.; White, C. T. *Phys. Rev. Lett*. **2002**, *89*, 285501. Holian, B. L.; Germann, T. C.; Maillet, J. B.; White, C. T. *Phys. Rev. Lett.* **2003**, *90*, 069902.

(11) Germann, T. C.; Holian, B. L.; Lomdahl, P. S.; Heom, A. J.; Gronbech-Jensen, N.; Maillet, J.-B. *Molecular Dynamics Simulations of Detonation in Defective Explosive Crystals*; Symposium of Detonation, 2002.

(12) Hatano, T. *Phys. Rev. Lett*. **2004**, *92*, 015503.

(13) Nomura, K.; Kali, R. K.; Nakano, A.; Vashishta, P. *Appl. Phys. Lett.* **2007**, *91*, 183109.

(14) Shi, Y. F.; Brenner, D. W. *J. Chem. Phys.* **2007**, *127*, 134503.

(15) Shi, Y. F.; Brenner, D. W. *Appl. Phys. Lett.* **2008**, submitted.